Soluble IGF2 Receptor Rescues *Apc*$^{Min/+}$ Intestinal Adenoma Progression Induced by *Igf2* Loss of Imprinting

James Harper,[1] Jason L. Burns,[1] Emily J. Foulstone,[1] Massimo Pignatelli,[1] Silvio Zaina,[2] and A. Bassim Hassan[1]

[1]Department of Cellular and Molecular Medicine, School of Medical Sciences, University of Bristol, Bristol, United Kingdom and
[2]Department of Clinical Biochemistry, Rigshospitalet, Copenhagen, Denmark

Abstract

The potent growth-promoting activity of insulin-like growth factor-II (IGF-II) is highly regulated during development but frequently up-regulated in tumors. Increased expression of the normally monoallelic (paternally expressed) mouse (*Igf2*) and human (*IGF2*) genes modify progression of intestinal adenoma in the *Apc*$^{Min/+}$ mouse and correlate with a high relative risk of human colorectal cancer susceptibility, respectively. We examined the functional consequence of *Igf2* allelic dosage (null, monoallelic, and biallelic) on intestinal adenoma development in the *Apc*$^{Min/+}$ by breeding with mice with either disruption of *Igf2* paternal allele or *H19* maternal allele and used these models to evaluate an IGF-II–specific therapeutic intervention. Increased allelic *Igf2* expression led to elongation of intestinal crypts, increased adenoma growth independent of systemic growth, and increased adenoma nuclear β-catenin staining. By introducing a transgene expressing a soluble form of the full-length IGF-II/mannose 6-phosphate receptor (sIGF2R) in the intestine, which acts as a specific inhibitor of IGF-II ligand bioavailability (ligand trap), we show rescue of the *Igf2*-dependent intestinal and adenoma phenotype. This evidence shows the functional potency of allelic dosage of an epigenetically regulated gene in cancer and supports the application of an IGF-II ligand–specific therapeutic intervention in colorectal cancer. (Cancer Res 2006; 66(4): 1940-8)

Introduction

New molecular markers of colorectal cancer risk and treatment are being identified, and one such common marker is epigenetic modification and loss of imprinting (LOI) of insulin-like growth factor 2 (*IGF2*), leading to increased ligand supply (1–4). LOI of *IGF2* is a commonly observed epigenetic abnormality in a wide range of other solid tumors in both human and murine models and is implicated as a potent modifier of cell growth and survival (5–10). Recent evidence suggests that ~10% of the human population may have LOI of *IGF2* in peripheral blood lymphocytes and normal colonic tissue, but in cases of colorectal cancer, the correlation with biallelic expression increases to 30%, with an odds ratio of >3.5 (11). There is little information concerning the intestinal, adenoma, or carcinoma phenotype that is generated by only a 2-fold increase in allelic dosage of *IGF2*. Two mechanisms seem to account for the LOI and are the basis of molecular tests: hypomethylation of a differentially methylated region (DMR) close to the *IGF2* coding region and hypermethylation of a CTCF binding region and DMR upstream of the noncoding *H19* promoter, resulting in disruption of an enhancer boundary (1, 3). In these circumstances, alterations in *IGF2* imprinting may simply reflect a bystander effect of global modification of DNA methylation that, in some circumstances, may be age related (12). However, direct functional information in the *Apc*$^{Min/+}$ mouse, a model of human intestinal polyposis, has shown that IGF-II supply directly modifies intestinal growth and promotes adenoma progression when continuously expressed using a bovine keratin 10 promoter driven transgene (5), and that biallelic expression of *Igf2* can increase adenoma burden (13).

IGF-II is a potent embryonic and tumor growth factor that signals via the IGF-I receptor (IGF1R) through the Ras/mitogen-activated protein kinase, phosphatidylinositol 3-kinase/Akt/FOXO, and S6K/mammalian target of rapamycin (mTOR) signaling pathways to modify cell proliferation, cell survival, gene expression, and cell growth (8, 9, 14). IGF-I, the related ligand, accounts for postnatal growth and persists throughout adult life, with levels in the high reference range being correlated with increased risk of prostate and breast cancer (15). IGF-II can activate signaling via the IGF1R, isoform A of the insulin receptor, and chimeric forms of the IR and IGF1R (16). Specific IGF1R kinase inhibitors, therapeutic antibodies to IGF1R and to both ligands, have been developed and seem to inhibit colorectal cancer cell growth (17, 18). Unlike IGF1R and IGF-binding proteins (IGFBP), IGF2R is a type I membrane protein that specifically binds IGF-II with high affinity (K_d = 10^{-10} mol/L) but does not lead to signal transduction (19). Rather, IGF2R functions to sequester IGF-II for internalization and degradation in the prelysosomal compartment and reflects its other main function as a mannose 6-phosphate receptor (19, 20).

Epigenetic modification and mutations of the IGF-II signaling system occur in human colorectal tumors (21). Supply of IGF-II is frequently up-regulated, and serial analysis of gene expression has shown *IGF2* as a commonly overexpressed gene in human colorectal cancer cell lines and tumors (22), and inactivating mutations of *IGF2R* and loss of heterozygosity are often detected in hereditary nonpolyposis colorectal cancer–derived tumors (23). Moreover, the proposed tumor suppressor function of *IGF2R* may also implicate other ligands, such as latent transforming growth factor-β1 (TGF-β1), which is activated once bound to the mannose 6-phosphate binding sites of the receptor (24). IGF-II supply is also a potent modifier of colorectal cancer cell line growth (21, 25, 26) and seems to be expressed in early colorectal adenoma (27).

Note: Supplementary data for this article are available at Cancer Research Online (http://cancerres.aacrjournals.org/).

Competing interests statement: The authors declare they have no competing financial interests.

Requests for reprints: A. Bassim Hassan, Department of Cellular and Molecular Medicine (formerly Pathology and Microbiology), School of Medical Sciences, University of Bristol, Bristol, BS8 1TD, United Kingdom. Phone: 44-117-928-7555; Fax: 44-117-928-7896; E-mail: Bass.Hassan@Bristol.ac.uk.

doi:10.1158/0008-5472.CAN-05-2036

In the mouse, *Igf2* and *Igf2r* are reciprocally imprinted and expressed from the paternal and maternal alleles, respectively (28–30). When detected with *in situ* hybridization, *Igf2* mRNA is normally detected during post-implantation development, with expression restricted to the paternal inherited allele in later development and in the adult, except in the exchange tissues of the brain (30). Disruption of the paternal allele ($Igf2^{+m/-p}$) results in proportional dwarfism first detected between E9.5 to E11, when quantified by either cell number or weight, respectively (31, 32). LOI of *Igf2* following maternal allele deletion of *H19* and a CTCF boundary element ($\Delta H19^{-m/+p}$) results in proportionate overgrowth that can be completely rescued by combination with $Igf2^{+m/-p}$, suggesting that loss of *H19* generates no other *Igf2*-independent effects (33).

Here, we quantify the specific functional consequences of the *Igf2* gene dosage in combination with the $Apc^{Min/+}$ model using $Igf2^{-m/-p}$ (homozygous null), $Igf2^{+m/-p}$ (maternal allele expressed alone), $Igf2^{+m/+p}$ (wild-type with paternal expressed allele intact), and $\Delta H19^{-m/+p}$ (biallelic expression). We then tested whether the phenotypes observed are due to increased ligand supply by the introduction of a bovine keratin 10–driven transgene expressing a soluble full-length mouse *Igf2r* (*K10ΔIgf2r*), previously shown to act as a ligand trap and to limit IGF-II bioavailability (23, 34–37).

Materials and Methods

Mice and genotyping. All experimental breeding was approved by local ethics committee and done under license from the U.K. Home Office. $Igf2^{+m/-p}$, $Apc^{Min/+}$, and $\Delta H19^{-m/+p}$ breeding pairs were obtained from Christopher Graham, Agiris Efstratiadis, Andrew Silver, and Shirley Tilghman and generated as described (30, 33, 38). Mice were housed, fed, and maintained as described previously in non–specific pathogen-free conditions (5). All mouse lines tested positive with PCR for stool *Helicobacter* species. Breeding schedules were as described (Table 1). DNA extraction from ear clips from 10-day-old mice and PCRs were done as previously described (5, 38), except for *H19*, which were genotyped using MutH19-For CTAGAGCTCGCTGATCAGCCT, MutH19-Rev GACAGTGGGAGTGGCACCTT, WtH19-For CCATCTTCATGGCCAACTCT, and WtH19-Rev AATGGGGAAACAGAGTCACG (annealing at 62°C).

Intestinal morphometry, adenoma scoring, and immunostaining. All animals were dissected at postnatal day 120, 1 hour after injection of bromodeoxyuridine (BrdUrd, 100 μg/g body weight). Small intestines and colons were opened, cleaned, and fixed in neutral buffered formalin as described (5). Whole mounts examined under a dissecting microscope were used to determine surface area and score adenoma number and size in the proximal, middle, and distal third of the small intestine, total colon, and cecum. H&E sections were blinded to genotype and used to quantify crypt depth (nuclei number), villus length (nuclei number), and pathologic grading. Colon epithelial tumors were confirmed by examination of sections. Counts of vertically aligned epithelial nuclei were obtained from 10 representative and intact crypts (from the base of crypt to the crypt-villus junction) and associated villi (from the crypt-villus junction to the tip of the villus) located in either the proximal, middle, and distal thirds of the small intestine, and 1 cm from the anorectal margin of the distal colon (five male mice per genotype). Pathologic grading was done blinded to genotype by (M.P., an experienced human and rodent gastrointestinal pathologist) and scored using established criteria in the mouse (39). Intestines from at least five mice per genotype were immunostained as described (5), except antigen retrieval was done by boiling in 10 mmol/L citric acid (5-20 minutes). Primary antibodies were against IGF1Rβ (3033, New England Biolabs, Beverly, MA), Ser^{473} phospho-Akt (9277, New England Biolabs), Ser^{256} phospho-FKHR (9461, New England Biolabs), E-cadherin (108, Santa Cruz Biotechnology, Santa Cruz, CA), Villin (7672, Santa Cruz Biotechnology), MCM2 (9839, Santa Cruz Biotechnology), Tyr^{632} phospho-IRS1 (17196, Santa Cruz Biotechnology), β-catenin (610154, Transduction, Lexington, KY) using BEAT blockade (Zymed, South San Francisco, CA), Lysosyme (DAKO, Carpinteria, CA), Muc2 (15334, Santa Cruz Biotechnology), and anti-BrdUrd (Roche, Indianapolis, IN). The proportion of epithelial cell nuclei stained with MCM2 was quantified using color digital images of at least 10 orientated crypt and villi using Image (NIH) software. The results expressed as a ratio of the number of nuclei from the base of the crypt to the level, where intense staining stops, relative to the total crypt-villus epithelial nuclei height.

RNA extraction and reverse transcription-PCR. For collection of tissue for reverse transcription-PCR (RT-PCR), tissues and adenoma were excised under a dissecting microscope, snap frozen in liquid nitrogen, and stored at −80°C. Total RNA was extracted using Trizol (Invitrogen, San Diego, CA), chloroform, and isopropanol precipitation. Following DNaseI treatment (Promega, Madison, WI), oligo-dT extraction (Promega), and reverse transcription, real-time PCR reactions with Taqman probes were done using a Stratagene MX3000P. For *Igf2* (NM_010514) and *Gapdh* (NM_008084), mouse Qiagen Quantitect Taqman probe assays (Chatsworth, CA) were used (241110 and 241012, respectively). For endogenous *Igf2r* (NM_010515), JHForward 5′-ACCTGTTCTCCTGGTACACTT-3′ and JHReverse 5′-CAGTAAGGCCAGCAAGCAG-3′ primers amplified product, which included the trans-membrane domain, and a Taqman probe-JHTaq

Table 1. Summary of mouse lines and genetic crosses

Cross	129S2 (abbreviated 129)		C57BL/6J (abbreviated B6)	
	Male	Female	Male	Female
1	*$Igf2^{+m/-p}$			†$Apc^{Min/+}$
2			‡$Igf2^{+m/-p}$, $Apc^{Min/+}$	‡$Igf2^{+m/-p}$, $Apc^{Min/+}$
3			$Apc^{Min/+}$	§$\Delta H19^{-m/+p}$
4	§*K10ΔIgf2r*/+			$Apc^{Min/+}$
5		§*K10ΔIgf2r*/+	‡$Igf2^{+m/-p}$, $Apc^{Min/+}$	
6	§*K10ΔIgf2r*/+			§$\Delta H19^{-m/+}$, $Apc^{Min/+}$

NOTE: 129S2$Igf2^{+m/tm1Rob\text{-}pat}$ ($Igf2^{+m/-p}$); C57Bl/6J$H19^{tm1Tilg}$ ($\Delta H19^{-m/+p}$); 129S2Tg(*K10ΔIgf2r*)kippsZai/+ (*K10ΔIgf2r*/+); C57Bl/6J$Apc^{Min/+}$ ($Apc^{Min/+}$).
*Inbred for >20 generations.
†Maintained line 1 C57Bl6/J $Apc^{Min/+}$ by breeding for five generations [total small intestinal adenoma number at 120 days for each generation 44 ± 11 (mean ± SD, n = 59)].
‡$Igf2^{+m/-p}$ crossed to parent C57Bl/67 for five generations before intercross.
§Inbred for >8 generations.

5′-FAM-TCCGCTCTGAGAGTCCTTTATACTCTGGCC-TAMRA-3′ were used for real-time product detection. For the *K10ΔIgf2r* transgene, primers JHForward and Reverse JHK10 5′-TCCCTTCTCTCCTTCTTACTAGT-3′, with the 3′ end corresponding to the inserted *Spe*I site in the deleted transmembrane region. JHTaq was also used to detect transgene expression, and RNA from an independent nontransgenic line was used as a negative control. Reactions were done for 40 cycles using Qiagen Quantitect reagents (204343) and following manufacturer's instructions (38, 40). Reaction conditions were initial denaturing, 94°C; annealing, 56°C; and extension for all experiments, 76°C. Additional positive and negative controls were cDNA from $Igf2^{+m/+p}$ and $Igf2^{-m/-p}$ mouse embryonic fibroblasts (passage 1) and plasmids with *Igf2r* and *K10ΔIgf2r* cDNA. Target gene quantification was done relative to *Gapdh* controls (normalized to 100,000 copies) using calibration reactions.

Statistical analysis. Comparisons between genotypes were displayed as box plots and used nonparametric statistics throughout (Mann Whitney, two tailed). Expected and observed breeding outcomes used χ^2 with Yates correction. Calculations used Minitab release 14.

Results

Allelic dosage of *Igf2* modifies intestinal growth and the crypt-villus axis. To quantify allelic dosage of *Igf2* on the $Apc^{Min/+}$ phenotype, we first did coisogenic (129/B6) and isogenic crosses (B6/B6) of inbred mouse lines to control for strain-dependent modifiers of $Apc^{Min/+}$ (41). $Igf2^{+m/-p}$ (null), $Igf2^{+m/+p}$ (monoallelic), and $\Delta H19^{-m/+p}$ (biallelic) were crossed with inbred $Apc^{Min/+}$ (Table 1). Increased allelic expression of *Igf2* resulted in increased intestinal growth by 120 days, as judged by overall surface area and crypt cell number (Fig. 1*A-B*; Supplementary Fig. S1; Supplementary Table S1). The effect of allelic dose did not seem uniform along the length of the small intestine and seemed more prominent in the proximal small intestine (Fig. 1*A*). Elongation of the crypt and villus proliferative zone was quantified using staining with an anti-MCM2 antibody that labels cells undergoing DNA replication (Fig. 1*C-D, MCM2*). Significant expansion of the proliferative zone was detected with increasing *Igf2* allelic dosage and was confirmed by anti-BrdUrd staining (data not shown). Differentiation of the small intestine was assessed using antibodies to E-cadherin, villin, MUC2, and lysosyme and only showed subtle attenuation of villin staining in $\Delta H19^{-m/+p}$, which seemed independent of altered intracellular distribution of β-catenin (Fig. 1*D*; Supplementary Fig. S2).

***Igf2* expression modifies intestinal signaling.** The distribution of IGF1R seemed independent of *Igf2* dosage (Fig. 1*D*). Specific ligand activation of the IGF1R was probed using a Tyr^{632} phospho-insulin receptor substrate-1 (phospho-IRS1) antibody, which detected signal in smooth muscle, intervillus stroma, and in a gradient extending from epithelial cells of the crypt to the villi (Fig. 1*D*). Little cytoplasmic labelling for phospho-IRS1 is visible in epithelial cells in sections from $Igf2^{+m/-p}$, except in the smooth muscle and stromal layers, presumably due to circulating IGF-I, and suggests that epithelial cell signal may be *Igf2* dependent (Fig. 1*D*). Similar distribution of cytoplasmic staining was detected with antibodies to phospho-Ser^{473} of Akt and phospho-Ser^{256} of FKHR (not shown). Quantitative RT-PCR using Taqman probes from control 120-day-old, 129, B6, and 129/B6 (data not shown) mice showed that *Igf2* mRNA is expressed in adult small intestine and colon at lower levels than in the heart, kidney, forestomach, and $Apc^{Min/+}$ adenoma, the latter confirming results from *in situ* hybridization (ref. 5; Fig. 2*A*). This evidence is supported by others (13) and refutes previous assumptions that *Igf2* expression is switched off in all adult mouse tissues. Moreover, *Igf2* mRNA is detectable in heart tissue at high levels, even in $Igf2^{+m/-p}$, indicating either loss of imprinting of *Igf2* in the heart, or high basal maternal allele expression (Fig. 2*A*). *Igf2* mRNA expression is globally increased in $\Delta H19^{-m/+p}$ but is not a direct 2-fold effect in most tissues at 120 days (Fig. 2*A*). There seems to be differences following comparison of *Igf2* expression between mouse strains (129 and B6) without disrupted *Igf2* supply. The magnitude of the increased expression in wild-type 129 compared with B6 is similar to comparison of wild-type B6 to $\Delta H19^{-m/+p}$ (B6/B6). Moreover, endogenous *Igf2r* expression on the 129 strain also seems higher than 129/B6 or B6/B6 expression (Fig. 2*B*), irrespective of expression of the *K10ΔIgf2r*/+ transgene (below, Fig. 2*C-D*). Overall, these observations suggest that continuous supply of ligand modifies crypt cell progenitor maturation independent of $Apc^{Min/+}$.

Allelic dosage of *Igf2* modifies $Apc^{Min/+}$ intestinal adenoma progression and dysplasia. Increased allelic *Igf2* dosage increased the total number of intestinal adenoma when genetically combined with $Apc^{Min/+}$ detected using dissection microscope examination of fixed intestinal whole mounts (mean ± SD): 10.4 ± 2.4 $Igf2^{+m/-p}$, $Apc^{Min/+}$ (null) versus 26.8 ± 7.4 $Igf2^{+m/+p}$, $Apc^{Min/+}$ (monoallelic), $P = 0.0002$ (129/B6) and 40.4 ± 22 $Igf2^{+m/+p}$, $Apc^{Min/+}$ (monoallelic) versus 58.8 ± 15.6 $\Delta H19^{-m/+p}$, $Apc^{Min/+}$ (biallelic), $P = 0.0097$ (B6/B6). However, when adenoma were normalized relative to growth of the small intestine and colon surface area, a significant decrease in total adenoma number was only detected in the small intestine of $Igf2^{+m/-p}$, $Apc^{Min/+}$ (129/B6, $P = 0.0002$), confirming our previous data obtained with lines contaminated with unknown $Apc^{Min/+}$ modifier alleles (ref. 5; Fig. 3*A*, normalized to intestinal growth). In comparison, a significant increase in normalized adenoma burden was only detected in $\Delta H19^{-m/+p}$, $Apc^{Min/+}$ (B6/B6) colon but not small intestine (Fig. 3*B*, normalized to colon growth). Inbreeding of $Igf2^{+m/-p}$ against the parent C57Bl6 line was done for five generations, before we attempted to generate complete $Igf2^{-m/-p}$, $Apc^{Min/+}$ (homozygous *Igf2* null mice) but failed to observe correct Mendelian segregation at birth (Supplementary Table S2). One $Igf2^{-m/-p}$, $Apc^{Min/+}$ (B6/B6) mouse survived into adulthood and had an adenoma burden equivalent to $Igf2^{+m/-p}$, $Apc^{Min/+}$ controls [129/B6, 0.58 versus 0.54 ± 0.12 (mean ± SD) adenoma cm^{-2}]. Distribution of small intestine adenoma size was similar between genotypes, except in $\Delta H19^{-m/+p}$, $Apc^{Min/+}$, where a disproportionate number seemed larger compared with wild-type $Apc^{Min/+}$ (Fig. 3*C*). Examination of adenoma sections, scored independently of genotype, revealed an increase in the proportion of adenoma containing at least a single focus of high-grade versus low-grade dysplasia in a mid-adenoma section of $\Delta H19^{-m/+p}$, $Apc^{Min/+}$ (68 of 85) versus $Apc^{Min/+}$ controls (12 of 22), confirming an effect of *Igf2* LOI on intestinal adenoma progression (Supplementary Fig. S3). Features of carcinoma *in situ* and stromal reaction were also detected in colonic adenoma from $\Delta H19^{-m/+p}$, $Apc^{Min/+}$, but no metastases were observed (Supplementary Fig. S3; ref. 39). Overall, this suggests that *Igf2* has predominant effects on adenoma progression when compared at a single time point (120 days), which seem to become more marked with increasing time.[3] Here, we cannot exclude modifier effects on adenoma initiation during crypt fission events in early intestinal development (42).

[3] Harper and Hassan, unpublished observations.

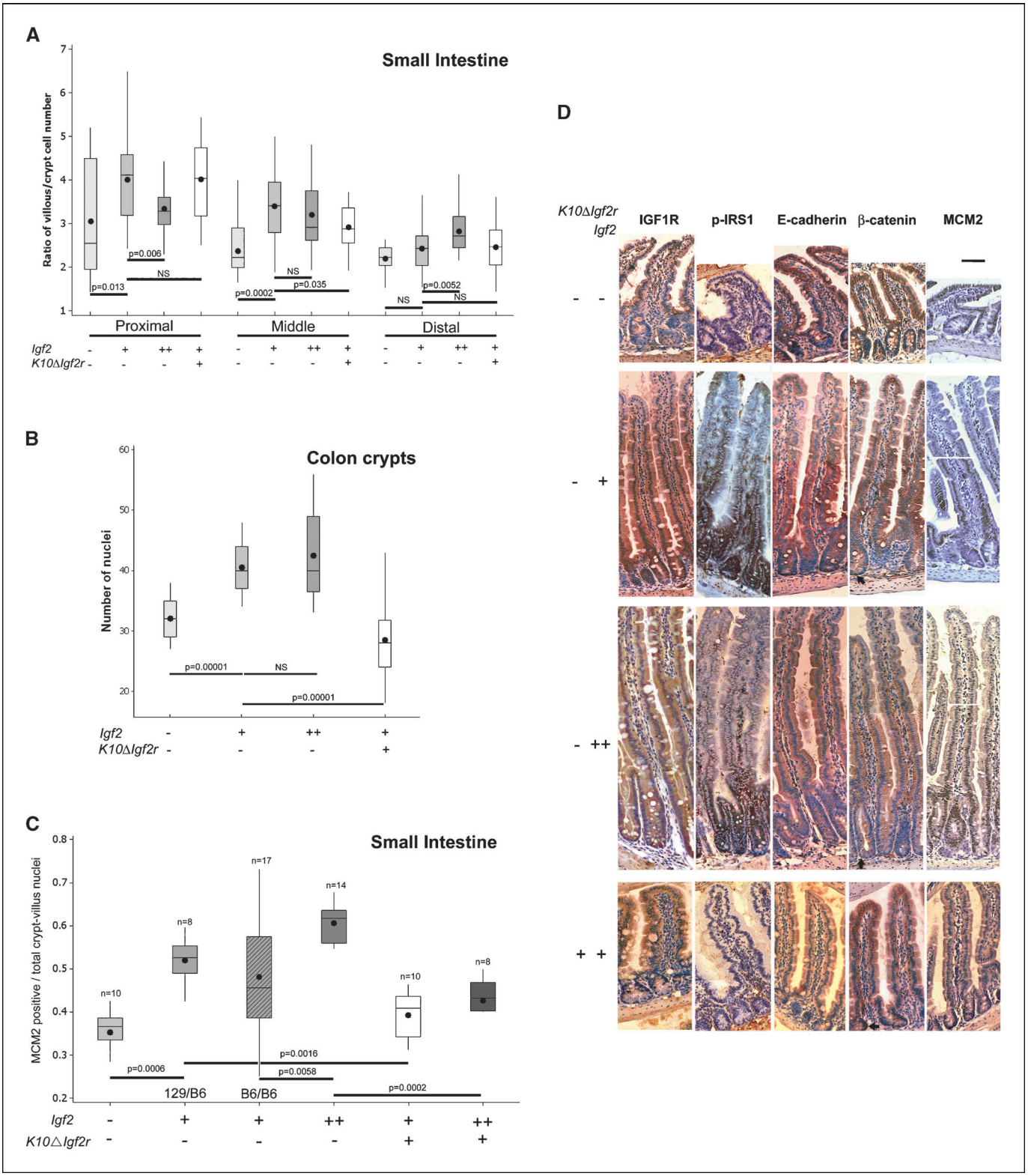

Figure 1. Morphometric analysis of *Igf2* allelic expression and intestinal growth. *A,* ratio of villus to crypt epithelial nuclei number (height) in the proximal, middle, and distal thirds of the small intestine. *Box,* interquartile range; *vertical line,* minimum to maximum value excluding outliers; *horizontal line,* median; *dot,* mean ($n = 50$ crypts and villi per genotype). *B,* height of distal colonic crypts expressed as nuclei number ($n = 50$ crypts per genotype). *C,* ratio of the number of MCM2-positive nuclei (height) from the crypt base up to where signal stops in the villi, relative to the total number of crypt and villi epithelial cell nuclei (proximal small intestine). *D,* representative small intestinal sections from 120-day-old mice stained with antibodies to IGF1-R, phospho-IRS1, E-cadherin, β-catenin, and MCM2 (brown/black staining). Note the elongation of biallelic *Igf2* small intestinal crypts and level of MCM2 staining (*white horizontal lines*), differential labelling of epithelial cells with phospho-IRS1 in $Igf2^{+m/-p}$ (note signal in smooth muscle but absence from epithelial cells) and *K10ΔIgf2r*/+ transgene intestine (see text), and no alteration in β-catenin distribution, with nuclear staining only in Paneth cells at the base of the crypts (*black arrows*). Bar, 100 μm. Genotypes for null *Igf2* expression $Igf2^{+m/-p}$ (−), monoallelic expression $Igf2^{+m/+p}$ (+), and biallelic expression $\Delta H19^{-m/+p}$ (++), with (+) and without (−) expression of a sIGF2R transgene *K10ΔIgf2r*/+. *NS,* not significant.

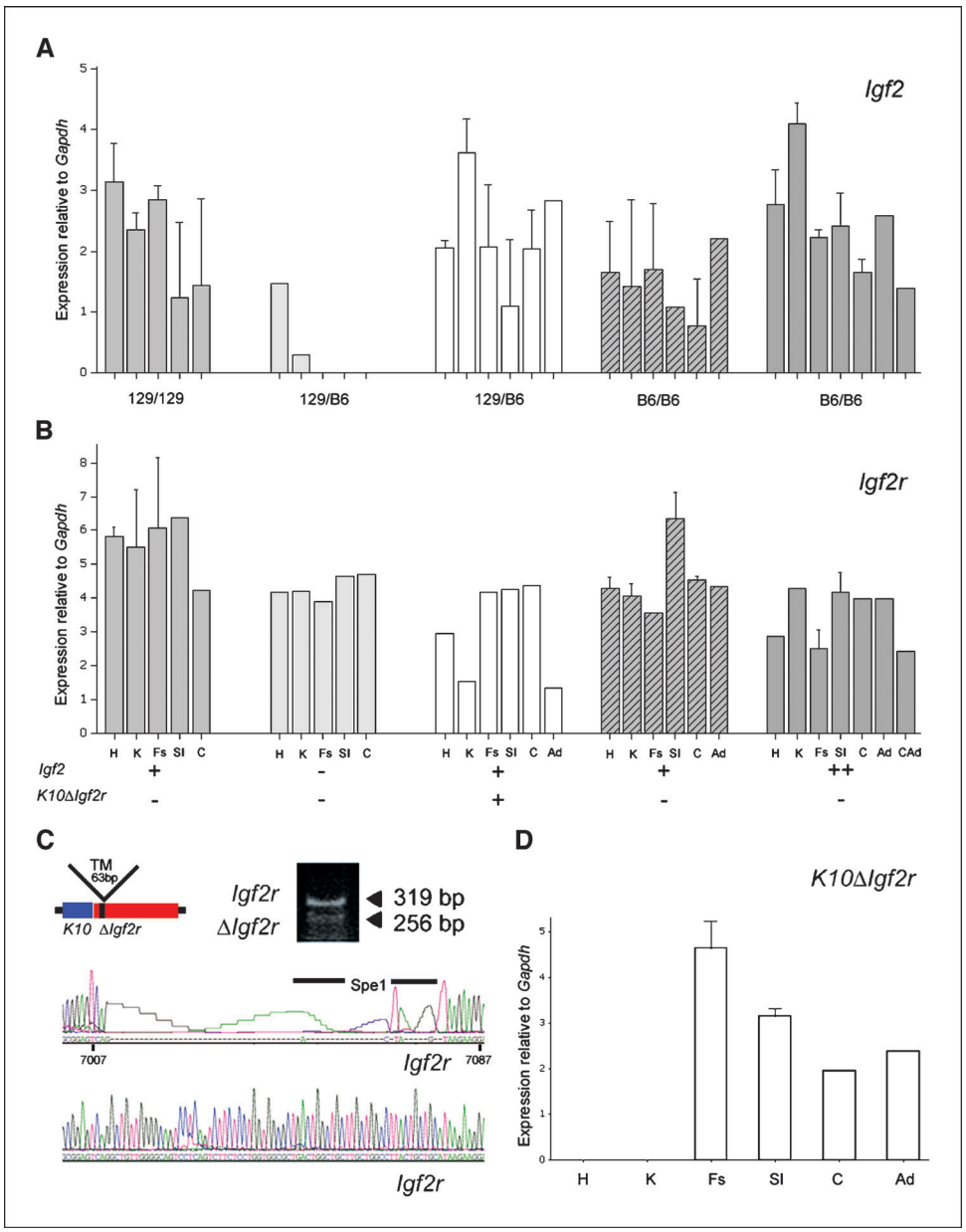

Figure 2. Analysis of *Igf2, Igf2r*, and *K10ΔIgf2r* mRNA expression in tissue and $Apc^{Min/+}$ intestinal adenoma. Tissue mRNA expression relative to *Gapdh* using Taqman quantitative RT-PCR for *Igf2* (*A*), *Igf2r* (*B*), and *K10ΔIgf2r*/+ transgene (*C* and *D*). Tissues [heart, *H*; kidney, *K*; forestomach, *Fs*; small intestine (proximal), *SI*; colon, *C*] and pooled adenoma ($n = 5$), except for *K10ΔIgf2r*/+ with only one adenoma, Ad (Colon Ad, CAd), were harvested from 120 day old mice [$Igf2^{+m/+p}$ ($n = 2$, 129/129), $Apc^{Min/+}$ combined with $Igf2^{+m/-p}$ ($n = 1$, 129/B6), $Igf2^{+m/+p}$ ($n = 2$, B6/B6), *K10ΔIgf2r*/+ ($n = 2$, 129/B6), and $\Delta H19^{-m/+p}$ ($n = 2$, B6/B6)]. *C,* ethidium-stained agarose gel example of RT-PCR amplification products of wild-type *Igf2r* and *K10ΔIgf2r*/+ transgene from forestomach tissue using primers 5′ and 3′ of the trans-membrane domain of *Igf2r* cDNA. DNA sequences of gel purified products confirm transgene expression with replacement of the *Igf2r* cDNA trans-membrane domain with a *Spe*I site. *D, K10ΔIgf2r*/+ transgene tissue specific expression (129/B6) using quantitative RT-PCR and Taqman transgene specific probes (see text).

Expression of a soluble IGF2R transgene rescues *Igf2* phenotypic effects in the intestine and in $Apc^{Min/+}$ adenoma. To confirm that effects of *Igf2* LOI were due to increased ligand supply, we evaluated a soluble form of IGF2R as a ligand-specific trap (36). In two independent bovine keratin 10 promoter-driven transgenic lines, sIGF2R reduced *Igf2*-dependent growth of intestinal tissues that expressed the transgene (129JS2, *K10ΔIgf2r*/+; refs. 34, 38). Heterozygotes of the highest expressing transgenic line (Kipps), expressed the transgene in the stomach, small intestine, colon, and adenoma, as detected by a transgene specific Taqman quantitative RT-PCR (Fig. 2*C-D*). In all cases, the transgene was transmitted from a 129 background in coisogenic crosses with B6 (129/B6). No circulating serum protein was detected with an IGF2R ELISA (data not shown), and endogenous *Igf2r* expression was not significantly affected by transgene expression (Fig. 2*B*). Crossing *K10ΔIgf2r*/+ with $Apc^{Min/+}$ (129/B6) resulted in a significant reduction of colonic crypt depth, MCM2 and phospho-IRS1 staining, and adenoma number to levels comparable with $Igf2^{+m/-p}$ (Fig. 1*B-D* and Fig. 3*A-C*; Supplementary Fig. S1 and Table S1). In particular, significantly less adenoma formed in the distal small intestine compared with $Apc^{Min/+}$ (*Igf2*, wild type) littermate controls ($P = 0.0003$; Fig. 3*A*). A second series of genetic crosses were used to evaluate *Igf2*-dependent and *Igf2*-independent effects of sIGF2R supply (Table 1). Combination of $Igf2^{+m/-p}$, $Apc^{Min/+}$ (B6/B6) with the transgene *K10ΔIgf2r*/+ (129/129, $n = 6$) resulted in no further reduction of adenoma number in the small intestine compared with $Igf2^{+m/-p}$, $Apc^{Min/+}$ controls ($n = 3$) and suggests that there is no significant *Igf2*-independent activity of sIGF2R (Fig. 4*A*). Combination of $\Delta H19^{-m/+p}$, $Apc^{Min/+}$ with the transgene also led to suppression of small intestinal MCM2 labeling (Fig. 1*C*), small intestine (Fig. 4*B*) and colonic (Fig. 4*C*) adenoma number, to levels equivalent to the *K10ΔIgf2r*/+, $Apc^{Min/+}$ controls despite limited mouse numbers, and confirmed the *Igf2*-dependent activity of *K10ΔIgf2r*/+ as a

specific inhibitor to the consequences of increased ligand supply generated by *Igf2* LOI. Moreover, the effects of transgene expression are independent of overall growth effects in the mouse, as determined by intestinal surface area and whole body weight (Supplementary Table S1).

Biallelic *Igf2* expression is associated with increased nuclear β-catenin staining. Unlike wild-type $Apc^{Min/+}$ small intestine and intestinal adenoma, where nuclear β-catenin was only detected in Paneth cells of the crypt (Fig. 1*D*), frequent presence of large regions of cytoplasmic and nuclear β-catenin were detected in sections through $\Delta H19^{-m/+p}$, $Apc^{Min/+}$ adenoma of all sizes (23 of 28 adenoma from mid-adenoma sections has at least one obvious focus, $n = 5$ mice) compared with littermate $Apc^{Min/+}$ controls (3 of 12, $n = 5$ mice; Fig. 4*D*). Staining of sections and Western blotting with E-cadherin antibodies failed to show significant down-regulation of E-cadherin in $\Delta H19^{-m/+p}$, $Apc^{Min/+}$ and suggests that the appearance of nuclear β-catenin is independent of E-cadherin activity (data not shown). In all adenoma, more extensive phospho-IRS1 labeling was also evident in areas, where there was nuclear β-catenin in $\Delta H19^{-m/+p}$, $Apc^{Min/+}$. Phospho-IRS1 staining seemed reduced in parallel processed specimens and was associated with a reduced extent of nuclear β-catenin staining in *K10ΔIgf2r/+*, $\Delta H19^{-m/+p}$, $Apc^{Min/+}$ adenoma, although persistence of staining was observed in adenoma that did only form in the proximal small intestine, presumably because of the differential extent of transgene expression in this region (Fig. 4*D*).

Discussion

A number of genetic mouse models with tumor susceptibility have been used to show the loss of *Igf2* expression and its

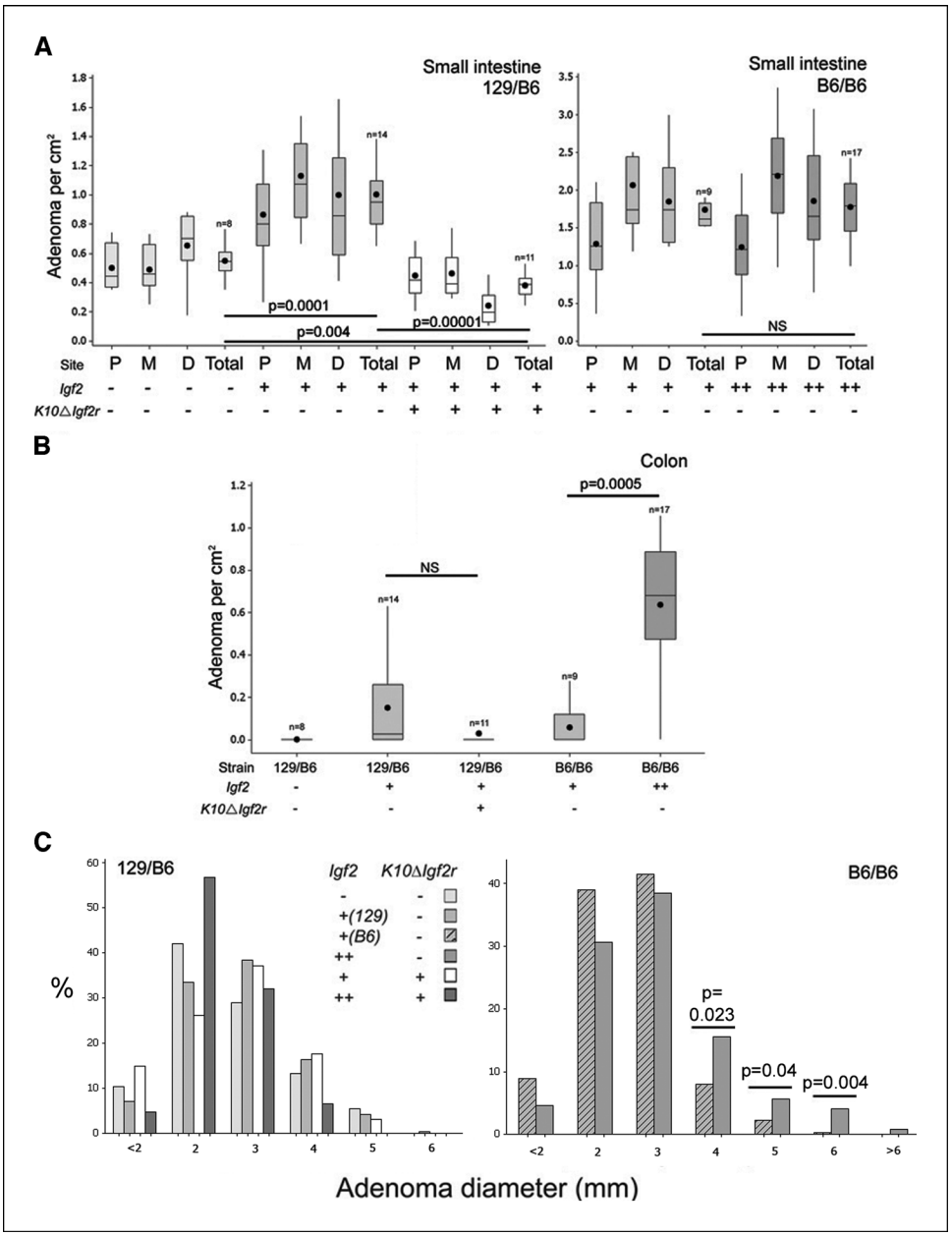

Figure 3. Analysis of *Igf2* allelic supply on $Apc^{Min/+}$ intestinal adenoma number and size. *A,* number of adenoma (corrected for surface area, cm^{-2}) for the proximal (*P*), middle (*M*), and distal (*D*) small intestine for the different genotypes of both 129/B6 coisogenic and B6/B6 isogenic crosses (see Table 1). Genotypes for null *Igf2* expression $Igf2^{+m/-p}$ (−), monoallelic expression $Igf2^{+m/+p}$ (+), and biallelic expression $\Delta H19^{-m/+p}$ (++), with (+) and without (−) expression of a sIGF2R transgene (*K10ΔIgf2r/+*). *B,* number of adenoma (corrected for surface area, cm^{-2}) for the colon as for (*B*). *C,* adenoma size (mm) percentage distributions for all mice counted in (*B*) separated for B6/129 and B6/B6 crosses (see *inset*). Significant increase in adenoma size is detected in $\Delta H19^{-m/+p}$ (++).

consequence to the progression of the tumor phenotype (5–8, 43, 44). In these circumstances, tumor size and frequency decrease and frequently reactivation of the normally silenced maternal allele of *Igf2* can occur (LOI). The mechanism of reactivation is presumed to be selection of epigenetically modified alleles that modify tumor cell survival, suggesting that activation of *Igf2* expression is essential for tumor progression in the mouse. Overexpression of either *Igf2* or *Igf1r* using transgenes results in local and systemic tumor formation when expressed at high levels alone and as a potent tumor promoter when combined with tumor-susceptible genetic models (5, 45, 46). However, the nonphysiologic expression in these circumstances limits the interpretation of these experiments.

Here, we show that biallelic expression of *Igf2* following germ line disruption of an imprinting control region upstream of *H19* results in marked intestinal phenotypic effects that seem independent of the generalized overgrowth phenotype (~130% of wild-type body weight). We then evaluated the consequences of this biallelic expression of *Igf2* on the development of the $Apc^{Min/+}$ intestinal adenoma phenotype and show that growth and differentiation effects seem to develop with increasing *Igf2* expression. In particular, we found that comparison of the expression of a single paternal allele of *Igf2* had significant effects on adenoma number as shown previously, whereas expression of both *Igf2* alleles resulted in no significant alteration in adenoma number in the small intestine, but an alteration in adenoma differentiation with associated high-grade dysplasia, and an increase in colonic adenoma number (5). Similar differential dose response effects of the IGF1R receptor in the RIPTag model have been described, with initial expression modifying tumor proliferation and apoptosis and higher expression associated with invasion and tumor metastasis (9). Results of a similar nature to those

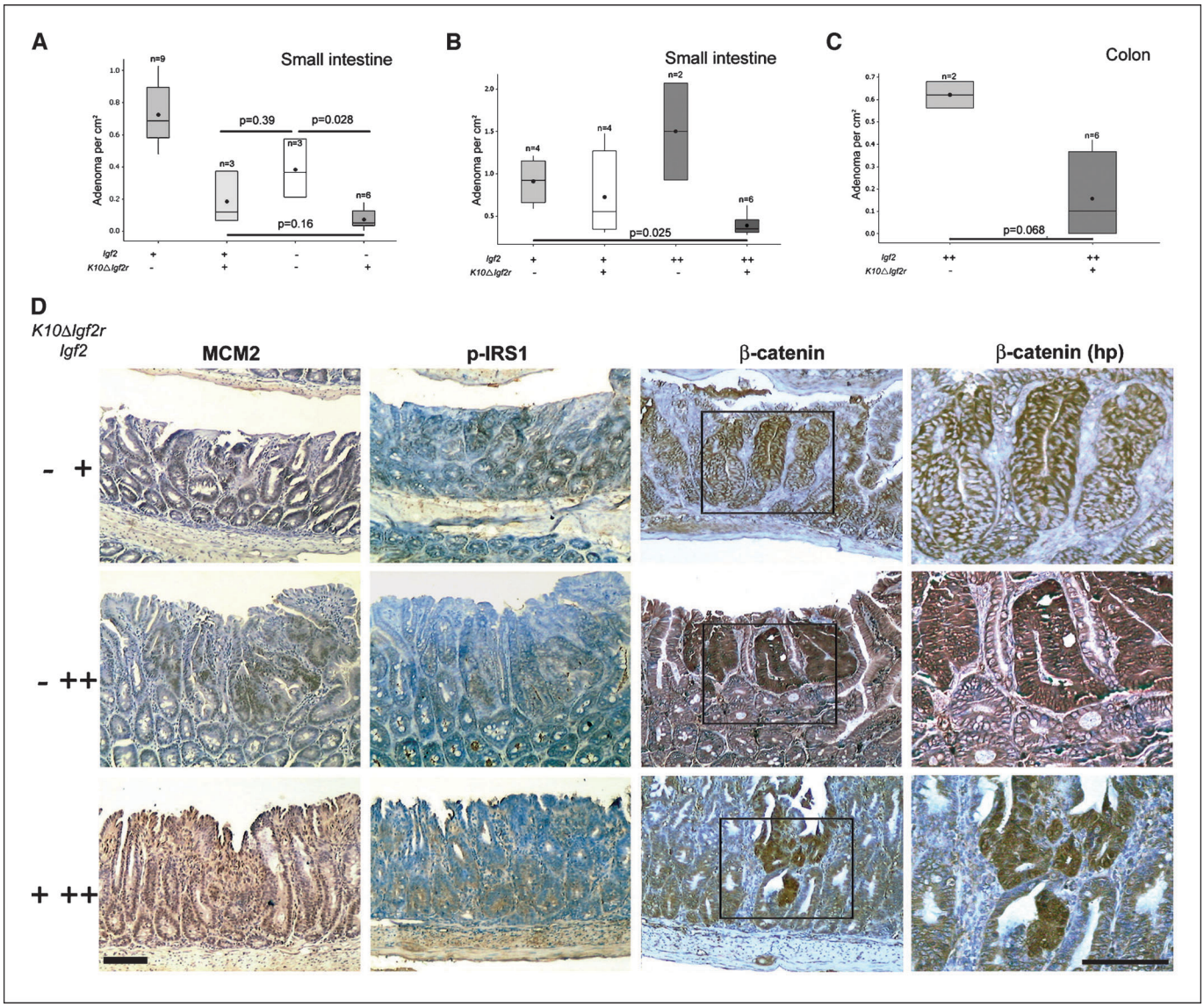

Figure 4. Analysis of *Igf2*-dependent and *Igf2*-independent activity of sIGF2R on $Apc^{Min/+}$ intestinal adenoma. Total number of adenoma (corrected for surface area, cm^{-2}) for littermates at postnatal day 120 in the small intestine following combination of genotypes $Igf2^{+m/-p}$, K10Δlgf2r/+, $Apc^{Min/+}$ (*A*) and $\Delta H19^{-m/+p}$, K10Δlgf2r/+, $Apc^{Min/+}$ (*B*, small intestine; *C*, colon). *D,* small intestinal adenoma stained with β-catenin, phospho-IRS1, and MCM2. Note the nuclear β-catenin in $\Delta H19^{-m/+p}$, $Apc^{Min/+}$ (++) and significant reduction of both epithelial nuclear β-catenin and phospho-IRS1 by expression of sIGF2R. Bar, 100 μm.

reported here have been obtained recently, and both are relevant to the observation that humans that develop colorectal cancer seem to frequently have systemic loss of imprinting leading to biallelic *Igf2* expression (2, 13). The data from Sakatani et al. (13) differ from those reported here, as we did not detect a significant increase in small intestinal adenoma number (when normalized for intestinal surface area) as a result of biallelic *Igf2* expression presumably because of the effects of strain-dependent $Apc^{Min/+}$ modifiers (13, 41). In this regard, although mRNA expression may not correlate with ligand supply, we note that global increases in relative *Igf2* expression were observed in wild-type 129 compared with B6 strain, suggesting that crosses containing 129 may have increased relative *Igf2* supply. In the context of $\Delta H19^{-m/+p}$, $Apc^{Min/+}$, although *Igf2* expression increases compared with $Apc^{Min/+}$ B6 controls, the eventual level of expression is only equivalent to that detected in the wild-type 129 line and may contribute to the differences in adenoma number between strains. However, the relative strain expression of *Igf2r* matches that of *Igf2*, and total adenoma number are lower in 129/B6 crosses than B6/B6, suggesting a more complex situation (see Figs. 2 and 3).

We directly tested the dose-dependent effect of *Igf2* allelic supply by expressing a soluble IGF2R expressing transgene, previously shown to inhibit overgrowth effects in the intestine generated as a consequence of IGF-II overexpression (34, 42, 47). Our results show rescue of the bialleic *Igf2* intestinal phenotype when combined with the $Apc^{Min/+}$ mouse, an effect which we also determined not to be independent of *Igf2* in parallel crosses with $Igf2^{+m/-p}$. This evidence suggests that the phenotypic effects observed are due to increased supply of ligand, as soluble IGF2R acts to limit IGF-II bioavailability. Previous studies in cell lines and tumors derived from them support the tumor suppressor function of membrane-bound and soluble IGF2R (35–37, 48). In some circumstances, excess supply of IGF2R may lead to increased conversion of latent TGF-β1 to active TGF-β1, but the results of genetic crosses fail to show any significant *Igf2*-independent activity in the small intestine and colon.

We propose that the reason that we observed an increase in adenoma number in the colon and adenoma growth in the small intestine was as a direct result of *Igf2* acting as a progression factor subsequent to the loss of initiating *Apc* tumor suppressor function (5, 8). The mechanism may be due to a combination of modification of cell survival, proliferation, growth, and differentiation. In addition, the mechanisms that underlie the modifier effects of *Igf2* allelic dosage on the intestinal adenoma phenotype implicate potential direct interactions between the *Igf2* and *Wnt* gene signaling systems. To date, evidence points towards modification of the bioavailability of β-catenin and phosphorylated substrates of Akt. One obvious target may be glycogen synthase kinase 3 (GSK3β), an Akt substrate and key modifier of Wnt signaling via phosphorylation of β-catenin. However, structural constraints exerted by Apc/Axin complexes negate functional interactions with Akt (49). Akt activation as a consequence of overexpression IGF1R mediated signaling seems to down-regulate the supply of E-cadherin, which also regulates cellular β-catenin, although we found no evidence to support this effect as a mechanism of nuclear β-catenin accumulation in adenoma (9, 50). Previous work suggests that IGF-II expression modifies colorectal cell differentiation and the nuclear localization of β-catenin (25, 26). In addition, expression of activated Akt can increase expression of luciferase reporter gene for β-catenin/Tcf (51). Recently, direct binding of β-catenin to FOXO transcription factors, phosphorylated and depleted from nuclei by IGF1R-and IR-mediated signaling, accounted for the increased activation of FOXO target genes (e.g., $p27^{Kip1}$) by increased nuclear β-catenin (52). Intriguingly, this evidence suggests that activated β-catenin would generate cell cycle arrest and apoptosis via direct activation of FOXO target genes, an effect that is inhibited and tumor promoting in the presence of IGF-II and Akt activation. If true, the marked effect of reduction in IGF-II supply in the context of activated β-catenin, as shown here in the context of $Apc^{Min/+}$, may be accounted for by β-catenin specifically sensitizing these cells to cell cycle arrest and cell death (52). Disruption of the FOXO target gene $p27^{Kip1}$ increases progression of $Apc^{Min/+}$, but not Smad3, intestinal adenoma, and is consistent with this hypothesis (53). Moreover, components of the IGF signaling pathway, such as mTOR and FOXO, may actually increase the rate of *Apc* loss of heterozygosity and increase adenoma-initiating events (54).

IGF-II ligand availability also seems to be modified by the β-catenin/Tcf–mediated overexpression of matrix metalloproteinase-7. Release of enzyme into the extracellular space then results in cleavage of IGFBP and increased local bioavailability of IGF-II ligand (55). The inhibitory consequences of *Mmp7* disruption on $Apc^{Min/+}$ adenoma is also consistent with this hypothesis but does not explain the apparent increase in *Igfbp5* expression in adenoma detected using expression arrays (56, 57). More importantly, the 2-fold effect of *Igf2* gene dosage would be normally omitted from array gene expression analysis and underscores the bias against potentially haploinsufficient gene phenotypes.

The potency of allelic dosage of *Igf2* is evident from the alteration in phenotype of the intestine crypt in the mouse, and this evidence supports the significant correlation between LOI of *Igf2* and the risk of developing sporadic colorectal cancer. Moreover, we have applied this validated genetic model to test potential therapeutic molecules that target this system. We tested the effects of a specific IGF-II intervention based on a soluble form of an endogenous receptor that normally functions to sequester IGF-II and is classed as a tumor suppressor. Similar use of ligand trap to other growth factors have been investigated in intestinal cancer (e.g., anti-vascular endothelial growth factor antibodies, soluble IGF1R, and soluble Noggin; refs. 58–60). A number of alternative approaches have also been developed to directly inhibit IGF ligand–mediated signaling, including IGF1R kinase inhibitors and antibodies directed at ligands and IGF1R (18, 58). We now provide genetic evidence that the consequences of excess supply of IGF-II ligand can be rescued by a specific high-affinity soluble IGF2 receptor, and this supports the rationale application of this novel IGF-II–targeted therapy for cancer.

Acknowledgments

Received 6/10/2005; revised 12/5/2005; accepted 12/13/2005.

Grant support: Cancer Research UK grant C429.

The costs of publication of this article were defrayed in part by the payment of page charges. This article must therefore be hereby marked *advertisement* in accordance with 18 U.S.C. Section 1734 solely to indicate this fact.

We thank Jenny Baker and Irene Withington for histology; Anne Hancock for quantitative PCR; Chris Graham (Department of Zoology, University of Oxford, Oxford, United Kingdom), Andrew Silver (St. Mark's Hospital, CR-UK, Harrow, United Kingdom), Wolf Reik (Babraham Institute, Cambridge, United Kingdom), Agiris Efstratiadis (Columbia University, New York, NY), and Shirley Tilghman (Princeton University, Princeton, NJ) for supply of mice; and Chris Graham and Chris Paraskeva for discussion.

References

1. Cui H, Onyango P, Brandenburg S, et al. Loss of imprinting in colorectal cancer linked to hypomethylation of H19 and IGF2. Cancer Res 2002;62:6442–6.
2. Cruz-Correa M, Cui H, Giardiello FM, et al. Loss of imprinting of insulin growth factor II gene: a potential heritable biomarker for colon neoplasia predisposition. Gastroenterology 2004;126:964–70.
3. Nakagawa H, Chadwick RB, Peltomäki P, et al. Loss of imprinting of the insulin-like growth factor II gene occurs by biallelic methylation in a core region of H19-associated CTCF-binding sites in colorectal cancer. Proc Natl Acad Sci U S A 2001;98:591–6.
4. Woodson K, Flood A, Green L, et al. Loss of insulin-like growth factor-II imprinting and the presence of screen-detected colorectal adenomas in women. J Natl Cancer Inst 2004;96:407–10.
5. Hassan AB, Howell JA. Insulin-like growth factor II supply modifies growth of intestinal adenoma in Apc(Min/+) mice. Cancer Res 2000;60:1070–6.
6. Haddad R, Held WA. Genomic imprinting and Igf2 influence liver tumorigenesis and loss of heterozygosity in SV40 T antigen transgenic mice. Cancer Res 1997;57:4615–23.
7. Hahn H, Wojnowski L, Specht K, et al. Patched target Igf2 is indispensable for the formation of medulloblastoma and rhabdomyosarcoma. J Biol Chem 2000;275:28341–4.
8. Christofori G, Naik P, Hanahan D. A second signal supplied by insulin-like growth factor II in oncogene-induced tumorigenesis. Nature 1994;369:414–8.
9. Lopez T, Hanahan D. Elevated levels of IGF-1 receptor convey invasive and metastatic capability in a mouse model of pancreatic islet tumorigenesis. Cancer Cell 2002;1:339–53.
10. Lamm GM, Christofori G. Impairment of survival factor function potentiates chemotherapy-induced apoptosis in tumor cells. Cancer Res 1998;58:801–7.
11. Cui H, Cruz-Correa M, Giardiello FM, et al. Loss of IGF2 imprinting: a potential marker of colorectal cancer risk. Science 2003;299:1753–5.
12. Issa JP, Vertino PM, Boehm CD, Newsham IF, Baylin SB. Switch from monoallelic to biallelic human IGF2 promoter methylation during aging and carcinogenesis. Proc Natl Acad Sci U S A 1996;93:11757–62.
13. Sakatani T, Kaneda A, Iacobuzio-Donahue CA, et al. Loss of imprinting of Igf2 alters intestinal maturation and tumorigenesis in mice. Science 2005;307:1976–8.
14. Foulstone E, Prince S, Zaccheo O, et al. Insulin-like growth factor ligands, receptors, and binding proteins in cancer. J Pathol 2005;205:145–53.
15. Renehan AG, Zwahlen M, Minder C, et al. Insulin-like growth factor (IGF)-I, IGF binding protein-3, and cancer risk: systematic review and meta-regression analysis. Lancet 2004;363:1346–53.
16. LeRoith D, Roberts CT, Jr. The insulin-like growth factor system and cancer. Cancer Lett 2003;195:127–37.
17. Miyamoto S, Nakamura M, Shitara K, et al. Blockade of paracrine supply of insulin-like growth factors using neutralizing antibodies suppresses the liver metastasis of human colorectal cancers. Clin Cancer Res 2005;11:3494–502.
18. Mitsiades CS, Mitsiades NS, McMullan CJ, et al. Inhibition of the insulin-like growth factor receptor 1 tyrosine kinase activity as a therapeutic strategy for multiple myeloma, other hematologic malignancies and solid tumours. Cancer Cell 2004;5:221–30.
19. Hassan AB. Keys to the hidden treasures of the mannose 6-phosphate/insulin-like growth factor 2 receptor. Am J Pathol 2003;162:3–6.
20. Ghosh P, Dahms NM, Kornfeld S. Mannose 6-phosphate receptors: new twists in the tale. Nat Rev Mol Cell Biol 2003;4:202–12.
21. Hassan AB, Macaulay VM. The insulin-like growth factor system as a therapeutic target in colorectal cancer. Ann Oncol 2002;13:349–56.
22. Zhang L, Zhou W, Velculescu VE, et al. Gene expression profiles in normal and cancer cells. Science 1997;276:1268–72.
23. Souza RF, Appel R, Yin J, et al. Microsatellite instability in the insulin-like growth factor II receptor gene in gastrointestinal tumours [letter]. Nat Genet 1996;14:255–7.
24. Dennis PA, Rifkin DB. Cellular activation of latent transforming growth factor beta requires binding to the cation-independent mannose 6-phosphate/insulin-like growth factor type II receptor. Proc Natl Acad Sci U S A 1991;88:580–4.
25. Morali OG, Delmas V, Moore R, et al. IGF-II induces rapid beta-catenin relocation to the nucleus during epithelium to mesenchyme transition. Oncogene 2001;20:4942–50.
26. Zarrilli R, Romano M, Pignata S, et al. Constitutive insulin-like growth factor-II expression interferes with the enterocyte-like differentiation of CaCo-2 cells. J Biol Chem 1996;271:8108–14.
27. Nosho K, Yamamoto H, Taniguchi H, et al. Interplay of insulin-like growth factor-II, insulin-like growth factor-I, insulin-like growth factor-I receptor, COX-2, and matrix metalloproteinase-7, play key roles in the early stage of colorectal carcinogenesis. Clin Cancer Res 2004;10:7950–7.
28. Lau MM, Stewart CE, Liu Z, et al. Loss of the imprinted IGF2/cation-independent mannose 6-phosphate receptor results in fetal overgrowth and perinatal lethality. Genes Dev 1994;8:2953–63.
29. Ludwig T, Eggenschwiler J, Fisher P, et al. Mouse mutants lacking the type 2 IGF receptor (IGF2R) are rescued from perinatal lethality in Igf2 and Igf1r null backgrounds. Dev Biol 1996;177:517–35.
30. DeChiara TM, Efstratiadis A, Robertson EJ. A growth-deficiency phenotype in heterozygous mice carrying an insulin-like growth factor II gene disrupted by targeting. Nature 1990;345:78–80.
31. Burns J, Hassan AB. Cell survival and proliferation are modified by Insulin-like growth factor II between days 9 and 10 of mouse gestation. Development 2001;128:3819–30.
32. Baker J, Liu JP, Robertson EJ, Efstratiadis A. Role of insulin-like growth factors in embryonic and postnatal growth. Cell 1993;75:73–82.
33. Leighton PA, Ingram RS, Eggenschwiler J, Efstratiadis A, Tilghman SM. Disruption of imprinting caused by deletion of the H19 gene region in mice [see comments]. Nature 1995;375:34–9.
34. Zaina S, Squire S. The soluble type 2 insulin-like growth factor (IGF-II) receptor reduces organ size by IGF-II-mediated and IGF-II-independent mechanisms. J Biol Chem 1998;273:28610–6.
35. Li J, Sahagian GG. Demonstration of tumor suppression by mannose 6-phosphate/insulin-like growth factor 2 receptor. Oncogene 2004;23:9359–68.
36. Scott CD, Ballesteros M, Madrid J, Baxter RC. Soluble insulin-like growth factor-II/mannose 6-P receptor inhibits deoxyribonucleic acid synthesis in cultured rat hepatocytes. Endocrinology 1996;137:873–8.
37. O'Gorman DB, Weiss J, Hettiaratchi A, Firth SM, Scott CD. Insulin-like growth factor-II/mannose 6-phosphate receptor overexpression reduces growth of choriocarcinoma cells *in vitro* and *in vivo*. Endocrinology 2002;143:4287–94.
38. Zaina S, Newton RV, Paul MR, Graham CF. Local reduction of organ size in transgenic mice expressing a soluble insulin-like growth factor II/mannose-6-phosphate receptor. Endocrinology 1998;139:3886–95.
39. Boivin GP, Washington K, Yang K, et al. Pathology of mouse models of intestinal cancer: consensus report and recommendations. Gastroenterology 2003;124:762–77.
40. Sansom OJ, Reed KR, Hayes AJ, et al. Loss of Apc *in vivo* immediately perturbs Wnt signaling, differentiation, and migration. Genes Dev 2004;18:1385–90.
41. Haines J, Johnson V, Pack K, et al. Genetic basis of variation in adenoma multiplicity in $Apc^{Min/+}$ Mom1S mice. Proc Natl Acad Sci U S A 2005;102:2868–73.
42. Bennett WR, Crew TE, Slack JM, Ward A. Structural-proliferative units and organ growth: effects of insulin-like growth factor 2 on the growth of colon and skin. Development 2003;130:1079–88.
43. Harris TM, Rogler LE, Rogler CE. Reactivation of the maternally imprinted IGF2 allele in TGFalpha induced hepatocellular carcinomas in mice. Oncogene 1997;16:203–9.
44. Christofori G, Naik P, Hanahan D. Deregulation of both imprinted and expressed alleles of the insulin-like growth factor 2 gene during beta-cell tumorigenesis. Nat Genet 1995;10:196–201.
45. Bates P, Fisher R, Ward A, et al. Mammary cancer in transgenic mice expressing insulin-like growth factor II (IGF-II). Br J Cancer 1995;72:1189–93.
46. Rogler CE, Yang D, Rossetti L, et al. Altered body composition and increased frequency of diverse malignancies in insulin-like growth factor-II transgenic mice. J Biol Chem 1994;269:13779–84.
47. Ward A, Bates P, Fisher R, Richardson L, Graham CF. Disproportionate growth in mice with Igf-2 transgenes. Proc Natl Acad Sci U S A 1994;91:10365–9.
48. Souza RF, Wang S, Thakar M, et al. Expression of the wild-type insulin-like growth factor II receptor gene suppresses growth and causes death in colorectal cancer cells. Oncogene 1999;18:4063–8.
49. Dajani R, Fraser E, Roe SM, et al. Structural basis for recruitment of glycogen synthase kinase 3beta to the axin-APC scaffold complex. EMBO J 2003;22:494–501.
50. Gottardi CJ, Wong E, Gumbiner BM. E-cadherin suppresses cellular transformation by inhibiting beta-catenin signaling in an adhesion-independent manner. J Cell Biol 2001;153:1049–60.
51. He XC, Zhang J, Tong WG, et al. BMP signaling inhibits intestinal stem cell self-renewal through suppression of Wnt-beta-catenin signaling. Nat Genet 2004;36:1117–21.
52. Essers MA, de Vries-Smits LM, Barker N, et al. Functional interaction between beta-catenin and FOXO in oxidative stress signaling. Science 2005;308:1181–4.
53. Philipp-Staheli J, Kim KH, Payne SR, et al. Pathway-specific tumor suppression. Reduction of p27 accelerates gastrointestinal tumorigenesis in Apc mutant mice, but not in Smad3 mutant mice. Cancer Cell 2002;1:355–68.
54. Aoki K, Tamai Y, Horiike S, Oshima M, Taketo MM. Colonic polyposis caused by mTOR-mediated chromosomal instability in Apc+/Delta716 Cdx2+/− compound mutant mice. Nat Genet 2003;35:323–30.
55. Miyamoto S, Yano K, Sugimoto S, et al. Matrix metalloproteinase-7 facilitates insulin-like growth factor bioavailability through its proteinase activity on Insulin-like growth factor binding protein 3. Cancer Res 2004;64:665–71.
56. Reichling T, Goss KH, Carson DJ, et al. Transcriptional profiles of intestinal tumors in Apc(Min) mice are unique from those of embryonic intestine and identify novel gene targets dysregulated in human colorectal tumors. Cancer Res 2005;65:166–76.
57. Wilson CL, Heppner KJ, Labosky PA, Hogan BL, Matrisian LM. Intestinal tumorigenesis is suppressed in mice lacking the metalloproteinase matrilysin. Proc Natl Acad Sci U S A 1997;94:1402–7.
58. D'Ambrosio C, Ferber A, Resnicoff M, Baserga R. A soluble insulin-like growth factor I receptor that induces apoptosis of tumor cells *in vivo* and inhibits tumorigenesis. Cancer Res 1996;56:4013–20.
59. Hurwitz H, Fehrenbacher L, Novotny W, et al. Bevacizumab plus irinotecan, fluorouracil, and leucovorin for metastatic colorectal cancer. N Engl J Med 2004;350:2335–42.
60. Haramis AP, Begthel H, van den Born M, et al. *De novo* crypt formation and juvenile polyposis on BMP inhibition in mouse intestine. Science 2004;303:1684–6.

Soluble IGF2 Receptor Rescues *Apc*$^{Min/+}$ Intestinal Adenoma Progression Induced by *Igf2* Loss of Imprinting

James Harper, Jason L. Burns, Emily J. Foulstone, et al.

Cancer Res 2006;66:1940-1948.